Dalton Transactions

Accepted Manuscript

ROYAL SOCIETY OF CHEMISTRY

www.rsc.org/dalton

Dalton Transactions RSCPublishing

ARTICLE

Theoretical study of the mechanism for the sequential N−O and N−N bond cleavage within N_2O adducts of *N*−heterocyclic carbenes by a vanadium(III) complex†

Cite this: DOI: 10.1039/x0xx00000x

Received 15th September 2015,
Accepted 00th November 2015

DOI: 10.1039/x0xx00000x

www.rsc.org/

Robert Robinson Jr.,[a] Miranda F. Shaw,[a] Robert Stranger,[b] and Brian F. Yates[a,*]

A theoretical study into the reactions of the N_2O adducts of *N*−heterocyclic carbenes (NHCs) and a $V^{(III)}$ complex was carried out using DFT calculations. Unlike most transition metal reactions with N_2O that simply release N_2 following O-atom transfer onto the metal centre, this NHC-based system traps the entire N_2O molecule and then cleaves both the N−O and N−N bond in two consecutive reactions. The NHC presence increases the reactivity of N_2O by altering the distribution of electron density away from the O-atom towards the two N-atoms. This electronic redistribution enables V−N binding interactions to form a reactive N,O-donor intermediate species. Our results show that bond breaking with concomitant ligand migration occurs *via* a concerted process for both the N−O and N−N cleavage reactions.

1. Introduction

Nitrous oxide (N_2O) is a severe greenhouse gas and has significant environmental impact as an ozone-depleting substance.[1] Indeed, its role also as an anthropogenic pollutant is becoming increasingly more apparent,[2] so that sequestering N_2O emissions has gained considerable attention. Most interest in N_2O chemistry has fixated on applications in organic syntheses, because of its high potential as an environmentally green oxidant, releasing N_2 as the sole by-product.[3] However, N_2O remains impractical in this capacity due to the fact that severe reaction conditions are necessary to surmount its strong inertness for bond activation. For example, even in the presence of a catalyst, the N_2O oxidation of benzene to phenol requires temperatures above 500 °C.[4] It is this high kinetic stability for bond cleavage that must be tackled to develop prospective N_2O reactions.

N_2O chemistry has been predominantly focused on exploiting metal complexes as promising activation agents to overcome this kinetic issue, despite its poor ligand properties (weak σ-donor and π-acceptor).[5] Coordination and activation is generally realised with electron-rich transition metals that are also capable of back-donation into the π^*-orbital (LUMO) of N_2O.[5a,6] In most instances, these metal-N_2O reactions simply cleave the weaker N−O bond *via* an O-atom transfer onto the metal centre followed by liberation of a N_2 molecule. However, the utilisation of N_2O as a N-atom transfer agent has only been realised in a few cases and rupture of the stronger N−N bond is exceedingly rare.[7]

Recently, it has emerged that certain frustrated Lewis pairs[8] and *N*−heterocyclic carbenes[9] (NHCs) are able to capture N_2O forming stable adducts under ambient conditions. Unlike most metal-N_2O complexes, these N_2O adducts display strong, covalent σ-bonds *via* the terminal N-atom and are remarkable in that they preserve the N_2O unit intact. Moreover, these NHC-N_2O adducts are also capable of undertaking further reactivity, such as thermolysis to form ureas (by N_2 release) or acid reactions to form guanidinium salts (by N−N bond cleavage).[9a,b]

An exciting finding is the reactivity between the N_2O adduct of 1,3-dimesitylimidazol-2-ylidene **(I^{Mes}–N_2O)** and $V(Mes)_3(THF)$ **(1−thf)**, as shown in Fig. 1.[9c] Because of the highly oxophilic nature of **1−thf**,[10] the anticipated O-atom transfer onto the V metal centre[11] was observed in the formation of the V−oxo product **2**. However, instead of releasing N_2, complex **2** contains a side-on bound I^{Mes}–N_2Mes diazo ligand that was reported as an insertion of the resulting I^{Mes}–N_2 species into a V−Mes bond.[9c] This reaction for forming **2** was observed to occur at room temperature. Also observed was a second reaction for the clean formation of the V−oxo product **3** upon heating **2** at 80 °C (Fig. 1), through N1−N2 bond scission and the additional Mes migration onto the former central N-atom (*N2*) of N_2O. This unusual system is quite distinct in that it utilises two reagents with complementary reactivity to divert the routine O-atom transfer and N_2 release. It is, therefore, an incentive to further examine *in silico* the interactions between **I^{Mes}–N_2O** and **1−thf** along with the reaction series that therein result.

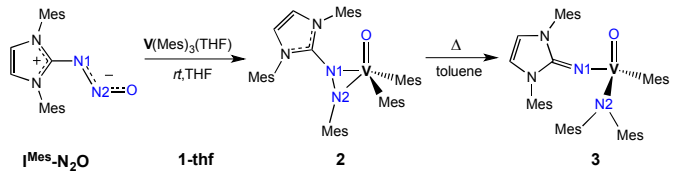

Fig. 1. Two reactions involving the deoxygenation of **I^{Mes}–N_2O** by **1−thf** (N−O rupture) in THF and the thermal-induced rearrangement of **2 → 3** (N−N rupture) in toluene.[9c]

Herein, we investigate the two reaction mechanisms by which cleavage of both the N−O and N−N bonds in N_2O are achieved in the unique reactivity between the N_2O adduct of 1,3-dimesitylimidazol-2-ylidene and $V(Mes)_3(THF)$. Notably, improving our knowledge of how a highly oxophilic metal centre interacts with the NHC-N_2O adduct and how a highly Lewis basic NHC weakens the N−N bond would be beneficial towards the understanding of the basic chemistry of N_2O activation.

2. Computational details

DFT calculations were performed with Gaussian09[12] at the M06[13] functional level utilising the integral equation formalism polarizable continuum model (IEF-PCM)[14] for either THF or toluene solvation. Optimised structures at the standard state (298.15 K and 1 atm) were located unrestricted and without symmetry constraints. The Stuttgart/Dresden double-ζ (SDD)[15] basis set with effective core potential (ECP) was used for the V-atom and the 6−31G(d)[16] basis set for other atoms, referred to as BS1. For optimisations of the $V(Ph)_3$ moieties, Ph ligands were initially positioned in an almost C_{3V}, propeller-like arrangement and afterwards, these structures were permitted to adopt their most favourable orientation for the Ph ligands. Frequency calculations were also performed at M06/BS1 to confirm the existence of minima or transition structures (TSs) based on the number of imaginary frequencies. For all TSs, the single imaginary frequency was visualised with GaussView[17] and intrinsic reaction coordinate (IRC)[18] calculations verified the connectivity between TSs and their relevant minima. Minimum energy crossing points (MECPs) were calculated with the code provided by J. Harvey *et al.*[19] at M06/BS1 and are reported uncorrected due to the absence of stationary points. To refine these results, single-point energies (SPEs) on optimised structures were performed using the Ahlrichs *et al.* quadruple-ζ (def2−QZVP)[20] basis set with SDD ECP for the V-atom and the 6−311+G(2d,p)[16] basis set on all other atoms, referred to as BS2. Natural bond orbital (NBO)[21] analysis was performed to evaluate the electronic population on each element within specified structures. Reported values are obtained from the thermal corrections to Gibbs energies at the M06/BS1 level and added to their corresponding SPEs, unless otherwise stated (see ESI† for an evaluation of the DFT methodology).

Structures are labelled as followed: (*i*) **N** (numbers) represent minima, **TS** transition structures and **TSB** bond-breaking TSs; (*ii*) **_X** (multiplicity) is denoted by **S** (singlet-state) or **T** (triplet-state); (*iii*) the Ph system is denoted by the **Ph** subscript, *e.g.* $\mathbf{N\_X_{Ph}}$; (*iv*) the NHC is abbreviated as $\mathbf{I^R}$ (imidazolium), where R represents the substituent groups on the N-atoms; and (*v*) the inverted orientation of $\mathbf{I^R–N_2O}$ is represented by an **i** script, *e.g.* **Ni_X** or $\mathbf{Ni\_X_{Ph}}$.

3. Results and discussion

Our theoretical study into the N−O and N−N bond cleavage reactions was carried out with substituents/ligands as either CH_3 or Ph groups. Preliminary calculations were performed with the less demanding CH_3 groups in order to efficiently utilise computational resources. This initial approach has performed quite well for our theoretical studies on other small molecule activations.[22]

3.1. NHC-N_2O adduct

As shown in Fig. 2, the N_2O adduct of 1,3-dimethylimidazol-2-ylidene **($\mathbf{I^{Me}–N_2O}$)** assumes a bent configuration of the N1−N2−O bond angle as compared to that in free N_2O (linear). This activation is also apparent as judged by the elongation of both N2−O and N1−N2 bonds in $\mathbf{I^{Me}–N_2O}$ to that calculated for free N_2O (1.181 and 1.132, respectively). Ideally, the N_2O fragment would remain coplanar with the NHC moiety to allow for optimal π-conjugation in the '*normal*' $\mathbf{I^{Me}–N_2O}$ orientation. However, an inverted orientation of $\mathbf{I^{Me}–N_2O}$ is also possible, in which the O-atom is rotated towards the NHC moiety (Fig. 2).

While the calculated stability for the inverted $\mathbf{I^{Me}–N_2O}$ is merely 13.1 kJ/mol higher than the *normal*, there is a moderate barrier for the intra-conversion between these two different orientations of $\mathbf{I^{Me}–N_2O}$ (Fig. 2). This result suggests that the inverted $\mathbf{I^{Me}–N_2O}$ is unlikely to be present in any significant concentration and is consistent with experimental findings as only *normal* NHC-N_2O species have been isolated.[9c]

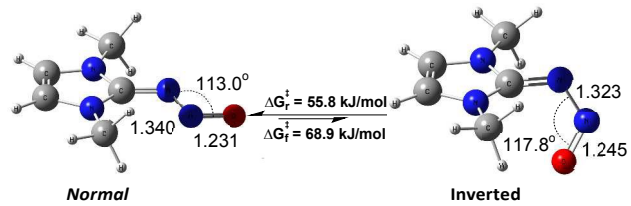

Fig. 2. Optimised structures of the *N*-nitrosoimine forms for $\mathbf{I^{Me}–N_2O}$ and the calculated intra-conversion between its two orientations. Selected bond lengths are in angstroms (Å) and bond angles are in degrees (°).

Interestingly, the presence of NHC within $\mathbf{I^{Me}–N_2O}$ increases the reactivity of N_2O by adjusting the electron density away from the O-atom towards the two N-atoms. Both NBO population analysis and Mulliken[23] atomic charges support this outcome. As shown in Table 1, the two N-atoms gain significantly more negative charge than that of the O-atom from the coordination of the Lewis basic NHC onto N_2O. This redistribution of electron density also allows all three atoms of the N_2O fragment to be potential donors (mesomeric $\mathbf{I^{Me}–N_2O}$ form, Fig. 1), unlike free N_2O. As a consequence, *normal* $\mathbf{I^{Me}–N_2O}$ would have several possible binding modes (O-, N- and chelating N,O-donor) onto a metal centre. Evidence of these $\mathbf{I^{Me}–N_2O}$ binding modes have been previously reported for various transition metals.[9a,c,24]

Table 1. NBO population analysis and Mulliken atomic charges[a]

	NBO			*Mulliken*		
	N1	N2	O	N1	N2	O
N_2O	-0.045	0.214	-0.169	-0.116	0.661	-0.545
$\mathbf{I^{Me}-N_2O}$	-0.241	0.068	-0.227	-0.421	0.086	-0.369

[a]N1 denotes the terminal N-atom of N_2O and N2 the central N-atom.

3.2. Vanadium complexation

The initial step is the reaction between *normal* $\mathbf{I^{Me}–N_2O}$ and the triplet $V(CH_3)_3(THF)$ complex **(1_T−thf)**, as its singlet **1_S−thf** lies 127 kJ/mol higher in energy. Thus, the reaction pathway for $V^{(III)}$ complexation will begin along the triplet-state surface, as the ground state of $\mathbf{I^{Me}–N_2O}$ is a singlet. As shown in Fig. 3, all possible

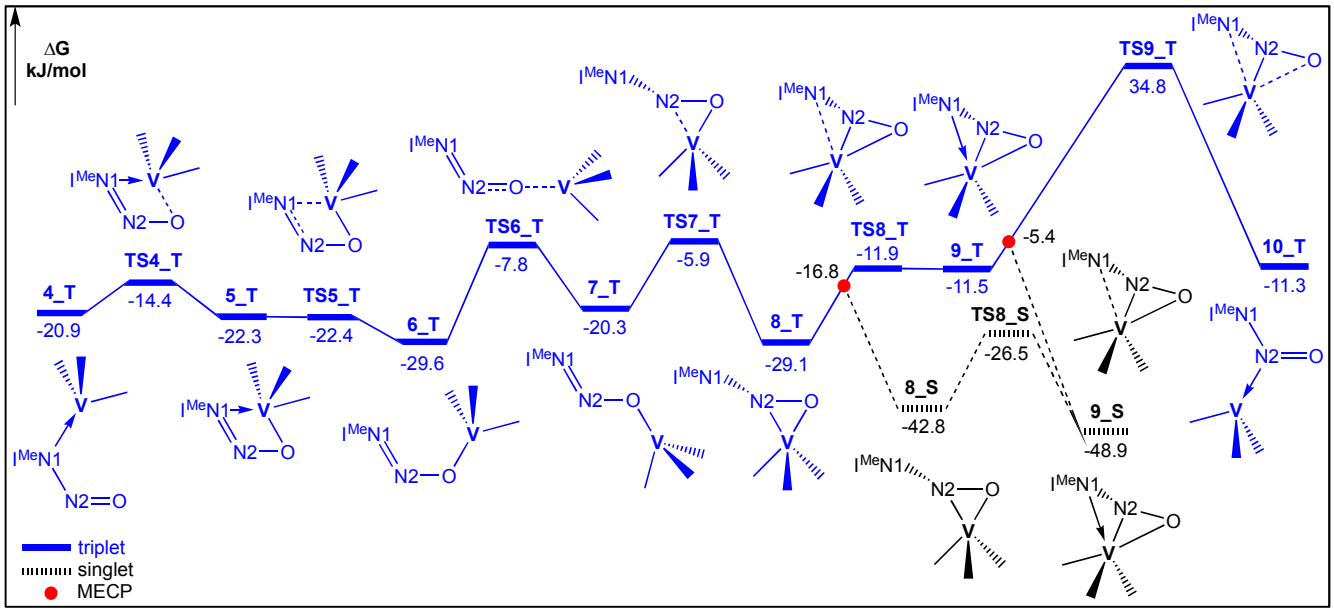

Fig. 3. Calculated profile for the formation of favourable *normal* I^{Me}-N_2O-$V(CH_3)_3$ complexes. All energies are relative to **1_T−thf** and *normal* $\mathbf{I^{Me}–N_2O}$ in THF.

$\mathbf{I^{Me}–N_2O}$ binding modes of the resulting I^{Me}-N_2O-$V(CH_3)_3$ complex were located along the triplet-state surface. The only exception is η^2–N1,N2 **(11_T)**, where all attempts to locate this structure led to formation of η^3–N1,N2,O **(9_T)**.

Along the triplet-state surface, each of these I^{Me}-N_2O-$V(CH_3)_3$ complexes were calculated to have favourable formations (negative ΔG) with η^1–O_{syn} **(6_T)** and η^2–N2,O **(8_T)** having greater stability (lower ΔG) than the other *normal* isomers (Fig. 3). The conversion processes towards more stable *normal* isomers were found to be quite feasible, ranging from barrierless to 38.2 kJ/mol. The possibility for intra-conversions of these *normal* isomers to their corresponding inverted isomers was also considered. However, such processes are unlikely to occur as the relative stabilities of all inverted isomers along the triplet-state surface (Table 2) lie above that of **6_T** and **8_T** (Fig. 3). The instability of the inverted isomers is attributed towards disruption of the *π*-conjugated system within the $\mathbf{I^{Me}–N_2O}$ moiety, *vide supra*.

Table 2. Calculated energies for selected I^{Me}-N_2O-$V(CH_3)_3$ complexes[a,b,c]

	Inverted				*Normal*		
	4i_T	7i_T	8i_T	10i_T	4_S	6_S	7_S
ΔG	-11.2	-1.7	-17.5	-15.7	99.4	51.8	50.6

[a]All ΔG energies (kJ/mol) are relative to **1_T−thf** and *normal* $\mathbf{I^{Me}–N_2O}$ in THF.
[b]**5i_T** and **6i_T** were not considered due to extensive steric hindrance.
[c]Attempts to locate **9i_T** led to formation of **8i_T**. Complex **10_S** led to the unobserved N−N insertion product, $(I^{Me}–N)V(CH_3)_3(NO)$.

For intersystem crossing (triplet→singlet), MECPs from the *normal* isomers: **8_T** and **9_T** were located and calculated to be energetically very small: 12.3 and 6.1 kJ/mol, respectively (Fig. 3). However, such intersystem crossings are unlikely to occur for the other triplet isomers. For example, a MECP from η^2–N1,O **(5_T)** is impossible as its singlet **5_S** is unstable and attempts to locate this led to formation of **8_S**. Also, spin-crossings from η^1–N1 **(4_T)**, **6_T** and η^1–O_{anti} **(7_T)** to form their relevant singlet isomers are unfavourable (ΔG >50 kJ/mol, Table 2).

Along the singlet-state surface, only two I^{Me}-N_2O-$V(CH_3)_3$ complexes were calculated to have favourable formations: **8_S** and **9_S**. Also, the conversion process between these singlet isomers was found to be quite feasible (≤22.4 kJ/mol, Fig. 3). Notably, these singlet isomers are more stable than their corresponding triplet isomers.

For **8_S** and **9_S**, their stability increase can be directly attributed towards pairing of the *d*-electrons, which leaves an unoccupied orbital on the V metal centre. Thus, the metal centre is allowed to accept further electronic donation from the N_2O fragment within $\mathbf{I^{Me}–N_2O}$ resulting in stronger interactions. This is evident from the shortening of both the V−N and V−O bond distances in **8_S** and **9_S** as compared to that in **8_T** and **9_T** (Fig. 4). This stabilising effect is further supported by the fact that η^1-coordinations of I^{Me}-N_2O-$V(CH_3)_3$ complex along the singlet-state surface are either unstable or unfavourable (Table 2).

Herein, it is noteworthy to mention that this stabilising effect was the only instance of a direct correlation between relative stabilities and their structures. No other structural trends relating to stability were identified among these isomers (see ESI† for calculated energies and selected bond lengths of all stable isomers). This result strongly implies that the stabilities of I^{Me}-N_2O-$V(CH_3)_3$ complexes are predominantly governed by electronic factors.

Additionally, the possibility for intra-conversions of **8_S** and **9_S** to their corresponding inverted isomers (**8i_S** and **9i_S**) was also considered. However, unlike the triplet isomers, such a process is only likely to occur for **9_S** and not for **8_S** (Fig. 4).

After $V^{(III)}$ complexation, only favourable isomers consisting of solely a V−O bond (**6_T** and **7_T**) are able to undergo an O-atom transfer from the $\mathbf{I^{Me}–N_2O}$ adduct. In such an event, an initial I^{Me}–N_2 would be formed without any further interaction with the V

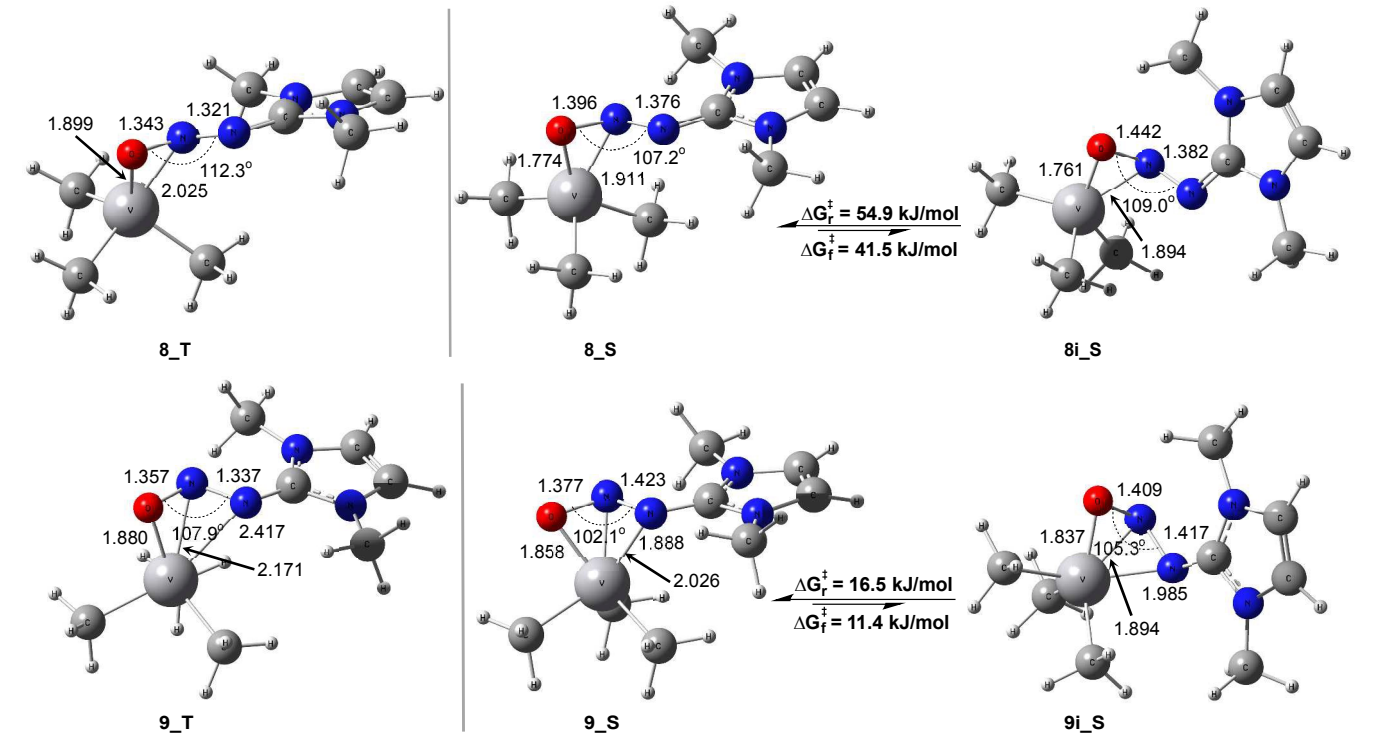

Fig. 4. Optimised structures of selected I^{Me}-N_2O-$V(CH_3)_3$ complexes along both surfaces. Selected bond lengths are in angstroms (Å) and bond angles are in degrees (°).

metal centre and eventually, releases I^{Me} and N_2 as the final products. However, such a process is not experimentally observed within this system.[9c] The unlikelihood for an O-atom transfer is further supported by the fact that **6_T** and **7_T** are calculated to have large reaction barriers: 90.4 and 59.8 kJ/mol, respectively (see ESI† for calculated bond cleavage reaction profiles along the triplet-state surface). Moreover, favourable isomers comprising of only a V−N bond (**4_T** and **10_T**) would most likely lead to conversions towards more stable $\mathbf{I^{Me}–N_2O}$ binding modes (Fig. 3).

3.3. N−O bond cleavage

The formation of the V−oxo product **2** from a I^{Me}-N_2O-$V(CH_3)_3$ complex requires N−O bond cleavage and a V-bound Mes ligand migration (Fig. 1). Only isomers comprising of both V−O and V−N bonds will be suitable for this concerted breaking/migration reaction.

Although the pathway begins along the triplet-state surface, these triplet isomers are not responsible for the formation of the V−oxo product **2**. For example, the breaking/migration reaction from **8_T** is calculated to have a large reaction barrier of 65.6 kJ/mol (see ESI† for calculated bond cleavage reaction profiles along the triplet-state surface). Furthermore, even though **5_T** and **9_T** are also capable of undergoing the breaking/migration reaction, both isomers have no barrier for conversion towards more stable $\mathbf{I^{Me}–N_2O}$ binding modes (Fig. 3). These results indicate that the breaking/migration reaction is impossible to initiate from a triplet isomer and must instead occur along the singlet-state surface.

Interestingly, both **8_S** and **9_S** exhibit stronger potential towards N_2O activation than their corresponding triplet isomers. This is apparent from the further elongation of the N2−O and N1−N2 bonds in **8_S** and **9_S** when compared to those in **8_T** and **9_T** (Fig. 4).

As shown in Fig. 5, the concerted breaking/migration reaction along the singlet-state surface shows two competitive pathways towards formation of **2_S**. The first reaction pathway from **8_S** proceeds through the anticipated O-atom transfer onto the V metal centre and a Me ligand migration on the N2-atom. This is calculated to have an activation energy of 25.2 kJ/mol *via* the bond-breaking transition structure **TSB8_S**. However, without the V−N1 bond interaction in **8_S**, an intermediate V−oxo species **(Int_S)** is initially formed, in which the N1-atom remains uncoordinated onto the V metal centre (Fig. 5). Afterwards, the V−N1 bond formation from **Int_S** is calculated to have a reaction barrier of 38.6 kJ/mol *via* **TSInt_S**, which leads to the V−oxo product **2_S**.

Unlike **8_S**, the second reaction pathway from **9_S** likely begins with the low-energy intra-conversion process towards **9i_S** (16.5 kJ/mol, Fig. 5), as all attempts to locate its bond-breaking transition structure **TSB9_S** led to formation of **TSB9i_S**. This result implies that as **9_S** proceeds towards the breaking/migration reaction it likely transforms into the less stable **9i_S**. In this instance, isomer **9i_S** has both V−N bonds present, so that only the O-atom transfer onto the V metal centre and a CH_3 migration onto the N2-atom are required to give **2_S**. This concerted breaking/migration reaction is calculated to have a reaction barrier of 33.3 kJ/mol *via* **TSB9i_S** (Fig. 5).

Irrespective of which pathway, the resulting small reaction barriers from both **8_S** and **9_S** are conducive with this breaking/migration process occurring at room temperature, which is consistent with the

experimental findings.[9c] In addition, the overall formation of the V−oxo product **2_S** is calculated to be a strongly exergonic process.

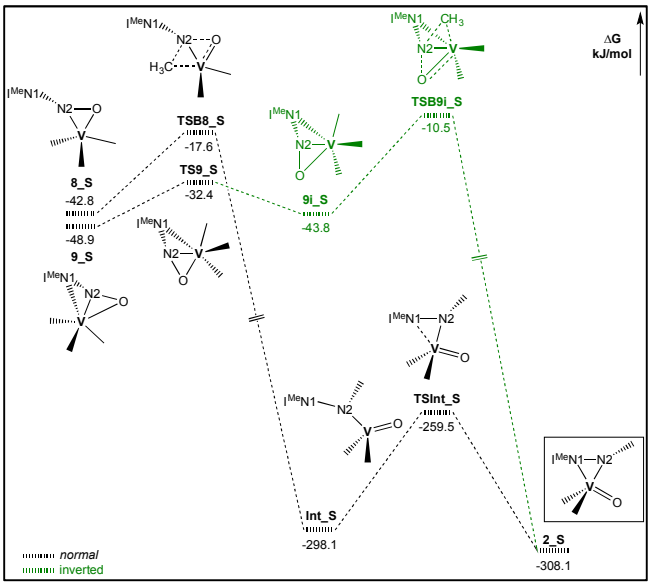

Fig. 5. Calculated reaction profiles for the N−O bond cleavage from η^2−N2,O **(8_S)** and η^3−N1,N2,O **(9_S)**. All energies are relative to **1_T−thf** and *normal* $\mathbf{I^{Me}}$**−N$_2$O** in THF.

Remarkably, upon closer inspection of **TSB8_S**, this bond-breaking transition structure exhibits an inverted $\mathbf{I^{Me}}$**−N$_2$O** fragment, which resembles that of **TSB9i_S** (Fig. 6). This structural rearrangement contributes towards the N−O bond cleavage by the metal centre, wherein the O-atom is 'forced' out-of-the-plane defined by the I^{Me}−N_2 fragment as the V metal shifts into this plane. This, in turn, opens a coordination site on the N2-atom – a necessity for the concomitant migration of an adjacent V-bound Me ligand. As a consequence, the **TSB8_S** structures adopt the inverted $\mathbf{I^{Me}}$**−N$_2$O** orientation, which is more favourable during the concerted breaking/migration reaction.

3.4. N−N bond cleavage

The formation of the V−oxo product **3** from **2** requires N−N bond cleavage and another V-bound Mes ligand migration (Fig. 1). This breaking/migration reaction is straightforward from **2_S**, wherein N1−N2 bond scission within the I^{Me}−N_2Me ligand is accompanied by a CH_3 migration onto the N2-atom (Fig. 7). This reaction pathway is well-demonstrated from a bond length analysis as judged by the lengthening of both N1−N2 and V−R′ bonds and shortening of the N2−R′ bond whilst proceeding from **2_S** towards **3_S** (Table 3). This concerted pathway is calculated to have a very high-energy reaction barrier *via* **TSB2_S**, which reflects the greater strength of the N1−N2 bond to that of the N2−O bond. This result is consistent with experimental findings, as heating of **2** at 80 °C in toluene is required for this reaction to proceed towards **3** (Fig. 1). Like **2_S**, the overall formation of **3_S** is also calculated to be a strongly exergonic process (Table 3).

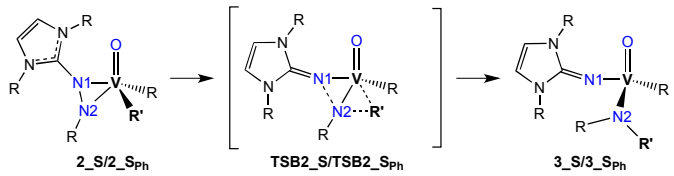

Fig. 7. Calculated reaction pathway for the N−N bond cleavage in toluene.

Of chemical significance, the formation of **3_S** demonstrates that NHC-activated N_2O can undergo N−N bond cleavage. Again, it is noteworthy to mention that this sort of reactivity for N_2O is exceedingly rare, *vide supra*.

Table 3. Calculated energies (kJ/mol) and selected bond lengths (Å) for **2_S/2_S$_{Ph}$ → 3_S/3_S$_{Ph}$**

	R = CH$_3$			*R = Ph*		
	2_S	**TSB2_S**	**3_S**	**2_S$_{Ph}$**	**TSB2_S$_{Ph}$**	**3_S$_{Ph}$**
ΔG	0.0	144.5	-201.9	0.0	148.2	-214.6
N1-N2	1.423	2.100	3.017	1.419	2.087	3.047
V-R′	2.046	2.188	2.958	2.035	2.116	3.005
N2-R′	2.755	2.337	1.444	2.779	2.545	1.406
V-N2	1.948	1.807	1.834	1.968	1.859	1.880

3.5. Comparison between CH$_3$ and Ph systems

In order to evaluate if the results from the CH_3 system are also operable for a more sterically demanding system, key structures along the low-energy reaction pathways (Fig. 5) were also calculated with Ph groups as the substituents/ligands.

As shown in Fig. 8, the Ph system demonstrates the identical competitive reaction pathways for N−O bond cleavage as that of the CH_3 system (Fig. 3). From **8_S$_{Ph}$**, the O-atom transfer and a Ph migration also led to an intermediate species **Int_S$_{Ph}$** and calculated to have a reaction barrier of 35.1 kJ/mol *via* **TSB8_S$_{Ph}$**. Afterwards,

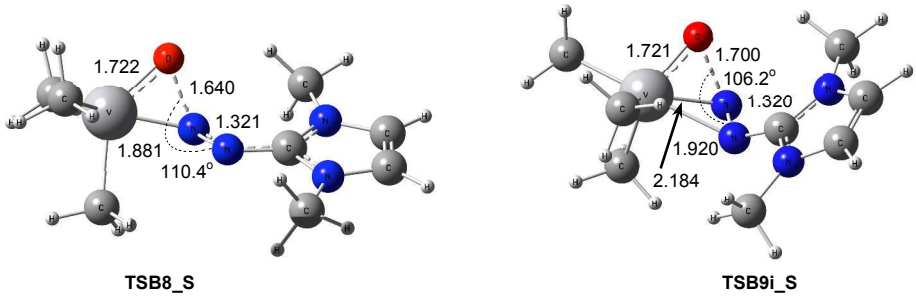

Fig. 6. Optimised structures of the bond-breaking transition structures **(TSB)** along the singlet surface. Selected bond lengths are in angstroms (Å) and bond angles are in degrees (°).

formation of the V−oxo product **2_S$_{Ph}$** is calculated to have an activation energy of 11.2 kJ/mol *via* **TSInt_S$_{Ph}$**. However, unlike the CH_3 system, the rate-determining step from **8_S$_{Ph}$** is the N−O bond cleavage. From **9i_S$_{Ph}$**, this concerted breaking/migration pathway is calculated to have a reaction barrier of 35.8 kJ/mol *via* **TSB9i_S** (Fig. 8).

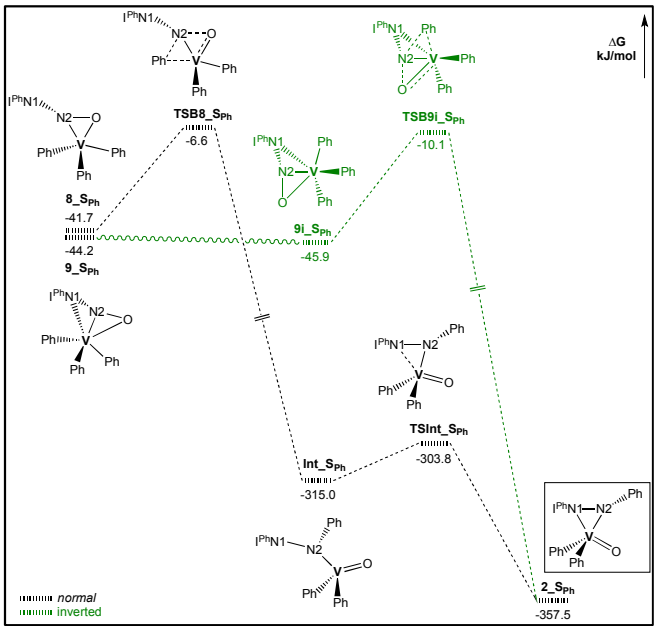

Fig. 8. Calculated reaction profiles for the N−O bond cleavage from η^2−N2,O **(8_S$_{Ph}$)** and η^3−N1,N2,O **(9_S$_{Ph}$)**. All energies are relative to **1_T$_{Ph}$−thf** and *normal* **I^{Ph}−N$_2$O** in THF.

The concerted breaking/migration for N−N bond cleavage within the Ph system also has an identical reaction pathway to that of the CH_3 system (Fig. 7). Also like the CH_3 system, the overall formations of both V−oxo products: **2_S$_{Ph}$** and **3_S$_{Ph}$** are calculated to be strongly exergonic processes (Fig. 8 and Table 3).

3.5. Conclusion

In summary, an I^{Mes}-activated N_2O adduct has been previously reported to cleave both the N−O and N−N bonds of the kinetically inert N_2O molecule when exposed to a V(Mes)$_3$(THF) complex. Such behaviour is considerably distinctive from that of most transition metal-induced N_2O interactions, in which simple N_2 is released following O-atom transfer onto the metal centre. The presence of the NHC within this system changes the expected reactivity of the N_2O by directly increasing the electron density on the N-atoms. As a result, the Lewis basicity of these N-atoms is also greatly increased, which allows them to strongly coordinate onto the metal centre. The importance of stronger N-atom interactions is that simple O-atom transfer is less likely to occur.

Our theoretical results show that these N−O and N−N cleavage reactions proceed through an initial VR_3 complexation onto the I^R−N_2O adduct that most likely forms a triplet-state N,O-donor isomer. Subsequently, this triplet I^R-N_2O-VR_3 complex will undergo intersystem crossing to give its more reactive singlet-state isomer. Then, N1−O bond cleavage combined with a ligand migration onto the N2-atom occurs *via* a small reaction barrier, resulting in a V−oxo product with a side-on bound I^R−N_2R diazo ligand on the V metal centre. Afterwards, N1−N2 bond cleavage also combined with another ligand migration onto the N2-atom occurs *via* a very high-energy reaction barrier. This resulting V−oxo product contains the remaining V-bound ligand (R), an amine (NR_2) and imidazolin-2-iminato ligands (I^R=N). Thus, our theoretical results for these concerted cleavage/migration reactions are in strong agreement with reported experimental findings.

The overall reactivity associated with the reactions discussed indicates that activated N_2O has the potential to be exploited as both an O- and N-atom transfer reagent. The crucial factor is provided by the influence of the NHC, which assists in stabilising the metal-N_2O adducts. Therefore, developing related metal complexes with electron-deficient centres for either stoichiometric and/or catalytic reactions would be a worthwhile goal for N_2O chemistry.

Acknowledgements

The authors would like to thank the Australian Research Council (ARC) for project funding through grant DP120101937. We also thank the National Computing Infrastructure (NCI) and Tasmanian Partnership for Advanced Computing (TPAC) for providing computational resources and technical support. M.F.S. acknowledges the financial support of an Australian Postgraduate Award.

Notes and references

[a]*School of Physical Sciences (Chemistry), University of Tasmania, Private Bag 75, Hobart, Tasmania 7001, Australia.*
E-mail: Brian.Yates@utas.edu.au; Fax: (+61) 3 6226 2858;
Tel: (+61) 3 6226 2167.
[b]*Research School of Chemistry, Australian National University, Canberra, ACT 0200, Australia.*

†Electronic Supplementary Information (ESI) available. See DOI: 10.1039/b000000x/

1. (*a*) Portmann, R. W.; Daniel, J. S.; Ravishankara, A. R. *Philos. Trans. R. Soc. London B: Biol. Sci.* **2012**, *367*, 1256-1267; (*b*) Dameris, M. *Angew. Chem. Int. Ed.* **2010**, *49*, 489-491; (*c*) Ravishankara, A. R.; Daniel, J. S.; Portmann, R. W. *Science* **2009**, *326*, 123-125; (*d*) Wuebbles, D. J. *Science* **2009**, *326*, 56-57.
2. Prather, M. J. *Science* **1998**, *279*, 1339-1341.
3. (*a*) Panov, G. I.; Dubkov, K. A.; Kharitonov, A. S. *Modern Heterogeneous Oxidation Catalysis*, Wiley-VCH, Weinheim, Germany **2009**, 217-252; (*b*) Parmon, V. N.; Panov, G. I.; Uriarte, A.; Noskov, A. S. *Catal. Today* **2005**, *100*, 115-131.
4. Iwamoto, M.; Hirata, J.; Matsukami, K.; Kagawa, S. *J. Phys. Chem.* **1983**, *87*, 903-905.
5. (*a*) Tolman, W. B. *Angew. Chem. Int. Ed.* **2010**, *49*, 1018-1024; (*b*) Lee, D. H.; Mondal, B.; Karlin, K. D. *Activation of Small Molecules*, Wiley-VCH, Weinheim, Germany **2006**, 43-79.
6. Yu, H.; Jia, G.; Lin, Z. *Organometallics* **2007**, *26*, 6769-6777.
7. (*a*) Cherry, J. P. F.; Johnson, A. R.; Baraldo, L. M.; Tsai, Y. C.; Cummins, C. C.; Kryatov, S. V.; Rybak-Akimova, E. V.; Capps, K. B.; Hoff, C. D.; Haar, C. M.; Nolan, S. P. *JACS* **2001**, *123*, 7271-7286; (*b*)

Laplaza, C. E.; Odom, A. L.; Davis, W. M.; Cummins, C. C.; Protasiewicz, J. D. *JACS* **1995**, *117*, 4999-5000.
8. (*a*) Neu, R. C.; Otten, E.; Lough, A.; Stephan, D. W. *Chem. Sci.* **2011**, *2*, 170-176; (*b*) Neu, R. C.; Otten, E.; Stephan, D. W. *Angew. Chem. Int. Ed.* **2009**, *48*, 9709-9712; (*c*) Otten, E.; Neu, R. C.; Stephan, D. W. *JACS* **2009**, *131*, 9918-9919.
9. (*a*) Tskhovrebov, A. G.; Vuichoud, B.; Solari, E.; Scopelliti, R.; Severin, K. *JACS* **2013**, *135*, 9486-9492; (*b*) Tskhovrebov, A. G.; Solari, E.; Wodrich, M. D.; Scopelliti, R.; Severin, K. *Angew. Chem. Int. Ed.* **2012**, *51*, 232-234; (*c*) Tskhovrebov, A. G.; Solari, E.; Wodrich, M. D.; Scopelliti, R.; Severin, K. *JACS* **2012**, *134*, 1471-1473.
10. (*a*) Tsai, Y. C.; Wang, P. Y.; Lin, K. M.; Chen, S. A.; Chen, J. M. *Chem. Commun.* **2008**, 205-207; (*b*) Cummins, C. C.; Schrock, R. R.; Davis, W. M. *Inorg. Chem.* **1994**, *33*, 1448-1457; (*c*) Bottomley, F.; Darkwa, J. *J. Chem. Soc., Dalton Trans.* **1988**, 2505-2506; (*d*) Bottomley, F.; Darkwa, J. *J. Chem. Soc., Dalton Trans.* **1983**, 399-400.
11. Palluccio, T. D.; Rybak-Akimova, E. V.; Majumdar, S.; Cai, X.; Chui, M.; Temprado, M.; Silvia, J. S.; Cozzolino, A. F.; Tofan, D.; Velian, A.; Cummins, C. C.; Captain, B.; Hoff, C. D. *JACS* **2013**, *135*, 11357-11372.
12. For the full *Gaussian09* reference, see the Electronic Supporting Information (ESI).
13. Zhao, Y.; Truhlar, D. G. *Acc. Chem. Res.* **2008**, *41*, 157-167.
14. Tomasi, J.; Mennucci, B.; Cammi, R. *Chem. Rev.* **2005**, *105*, 2999-3094.
15. Andrae, D.; Häußermann, U.; Dolg, M.; Stoll, H.; Preuß, H. *Theoret. Chim. Acta* **1990**, *77*, 123-141.
16. Hariharan, P. C.; Pople, J. A. *Theoret. Chim. Acta* **1973**, *28*, 213-222.
17. Dennington, R. D.; Kieth, T. A.; Millam, J. M. *GaussView5.0, Semichem, Inc.*: Shawnee Mission, KS **2009**.
18. (*a*) Fukui, K. *Acc. Chem. Res.* **1981**, *14*, 363-368; (*b*) Fukui, K. *J. Phys. Chem.* **1970**, *74*, 4161-4163.
19. Harvey, J. N.; Aschi, M.; Schwarz, H.; Koch, W. *Theor. Chem. Acc.* **1998**, *99*, 95-99.
20. Weigend, F.; Furche, F.; Ahlrichs, R. *J. Chem. Phys.* **2003**, *119*, 12753-12762.
21. Glendening, E. D.; Reed, A. E.; Carpenter, J. E.; Weinhold, F. *NBO ver. 3.1, Gaussian, Inc.*: Pittsburgh, PA **2003**.
22. (*a*) Robinson, R.; Abbasi, K. K.; Ariafard, A.; Stranger, R.; Yates, B. F. *Inorg. Chem.* **2015**, *54*, 534-543; (*b*) Shaw, M. F.; Mahdizadeh Ghohe, N.; Ariafard, A.; Brookes, N. J.; Stranger, R.; Yates, B. F. *Dalton Trans.* **2014**, *43*, 1620-1629; (*c*) Cavigliasso, G.; Criddle, A.; Kim, H. S.; Stranger, R.; Yates, B. F. *Dalton Trans.* **2014**, *43*, 4631-4634; (*d*) Cavigliasso, G.; Stranger, R.; Yates, B. F. *Dalton Trans.* **2012**, *41*, 13948-13959; (*e*) Cavigliasso, G.; Christian, G. J.; Stranger, R.; Yates, B. F. *Dalton Trans.* **2011**, *40*, 7327-7339; (*f*) Ariafard, A.; Brookes, N. J.; Stranger, R.; Yates, B. F. *Organometallics* **2011**, *30*, 1340-1349; (*g*) Ariafard, A.; Brookes, N. J.; Stranger, R.; Boyd, P. D. W.; Yates, B. F. *Inorg. Chem.* **2010**, *49*, 7773-7782; (*h*) Cavigliasso, G.; Wilson, L.; McAlpine, S.; Attar, M.; Stranger, R.; Yates, B. F. *Dalton Trans.* **2010**, *39*, 4529-4540. (*i*) Christian, G.; Stranger, R.; Yates, B. F.; Cummins, C. C. *Dalton Trans.* **2007**, 1939-1947.
23. (*a*) Mulliken, R. S. *J. Chem. Phys.* **1955**, *23*, 1833-1840; (*b*) Mulliken, R. S. *J. Chem. Phys.* **1955**, *23*, 1841-1846; (*c*) Mulliken, R. S. *J. Chem. Phys.* **1955**, *23*, 2338-2342; (*d*) Mulliken, R. S. *J. Chem. Phys.* **1955**, *23*, 2343-2346.
24. Tskhovrebov, A. G.; Solari, E.; Scopelliti, R.; Severin, K. *Inorg. Chem.* **2013**, *52*, 11688-11690.

Dalton Transactions RSCPublishing

ARTICLE

Table of Contents graphic

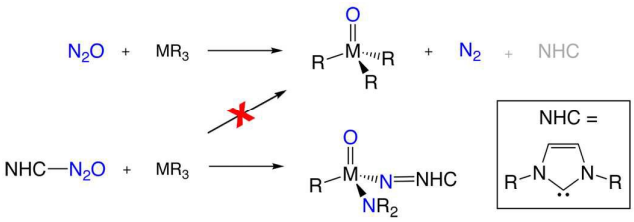

The addition of *N*-heterocyclic carbene (NHC) increases the activity of N_2O towards cleavage of both the N−O and N−N bonds.